11728–11736 *Nucleic Acids Research, 2012, Vol. 40, No. 22* *Published online 16 October 2012*
doi:10.1093/nar/gks953

Direct quantitative analysis of HCV RNA by atomic force microscopy without labeling or amplification

Yu Jin Jung[1,*], Jeffrey A. Albrecht[2], Ju-Won Kwak[3] and Joon Won Park[3,*]

[1]Nanogea Corporation, 6162 Bristol Parkway, Culver City, CA 90230, USA, [2]National Genetics Institute, 2440 S. Sepulveda Blvd. Suite #235, Los Angeles, CA 90064, USA and [3]Department of Chemistry, Division of Integrative Biosciences and Biotechnology, Pohang University of Science and Technology, San 31 Hyoja-dong, Pohang 790-784, South Korea

Received August 5, 2012; Revised September 19, 2012; Accepted September 20, 2012

ABSTRACT

Force-based atomic force microscopy (AFM) was used to detect HCV (hepatitis C virus) RNA directly and to quantitatively analyse it without the need for reverse transcription or amplification. Capture and detection DNA probes were designed. The former was spotted onto a substrate with a conventional microarrayer, and the latter was immobilized on an AFM probe. To control the spacing between the immobilized DNAs on the surface, dendron self-assembly was employed. Force–distance curves showed that the mean force of the specific unbinding events was 32 ± 5 pN, and the hydrodynamic distance of the captured RNA was 30–60 nm. Adhesion force maps were generated with criteria including the mean force value, probability of obtaining the specific curves and hydrodynamic distance. The maps for the samples whose concentrations ranged from 0.76 fM to 6.0 fM showed that cluster number has a linear relationship with RNA concentration, while the difference between the observed number and the calculated one increased at low concentrations. Because the detection limit is expected to be enhanced by a factor of 10 000 when a spot of 1 micron diameter is employed, it is believed that HCV RNA of a few copy numbers can be detected by the use of AFM.

INTRODUCTION

Significant progress in genome and proteome studies for disease diagnosis and prevention has created a strong demand for advanced biomolecular detection with high sensitivity and specificity (1–5). In particular, early diagnosis is important in cancer and other pathologies because treatment of such diseases at an early stage improves the survival rate (6). Therefore, nanotechnology enhancing biomolecular detection is one of the most rewarding fields. The hepatitis C virus (HCV) is a small, enveloped, single-stranded, positive-sense RNA virus whose length is 9.6 kilobases (kb) (7,8). It is the only known member of the *Hepacivirus* genus in the *Flaviviridae* family. HCV is one of the most important causes of chronic liver disease worldwide, and 3% of the world's population is estimated to be infected (7,9–12). Hepatitis C is rarely diagnosed during the acute phase of the disease, partly because the majority of people infected experience no symptoms during this phase (11,13). Moreover, those who do experience acute phase symptoms are rarely ill enough to seek medical attention. Untreated HCV induces chronic infection in 50–80% of infected persons and chronic HCV infection leads to cirrhosis in about 10–20% of patients, increasing the risk of complications of chronic liver disease, including portal hypertension, ascites, hemorrhage and hepatocellular carcinoma (14–17). To diagnose acute hepatitis C, serologic screening alone is insufficient because anti-HCV antibodies may develop late after transmission of the virus (18–20). In contrast, HCV RNA is detectable within a few days of infection, so HCV RNA tests are important clinical tools for diagnosing HCV infection and guiding its treatment.

To check for the presence of HCV RNA and measure the amount of the HCV RNA virus, the corresponding RNA is converted into DNA by reverse transcription. Amplification is typically achieved by polymerase chain reaction (PCR) (11,21) or transcription-mediated amplification (TMA) (22,23), or by using branched DNA (b-DNA) (24,25). In addition to the lengthy steps needed, the use of fluorescent dyes, PCR errors, the presence of polymerase inhibitor in blood and tissues, and amplification failure are examples of the drawbacks of these methods (26–28). Thus, finding an approach in which RNA is measured directly is desirable, thereby reducing the errors that occur during the multistep treatment.

*To whom correspondence should be addressed. Tel: +82 54 279 2119; Fax: +82 54 279 0635; Email: jwpark@postech.ac.kr
Correspondence may also be addressed to Yu Jin Jung. Tel: +1 310 649 5600; Email: yjung@nanogea.com

Here, we offer a new adhesion force mapping-based approach using atomic force microscopy (AFM) to measure RNA directly and overcome the limitations of the current approaches. Recently, force-based AFM has been widely employed in biological areas because it is compatible with non-conductive materials, does not require labeling, and can be operated under physiological conditions, while allowing single molecule analysis and achieving enhanced detection limits (29–35). To make the analysis more reliable and reproducible, the surface is modified with a nanostructured macromolecule called a dendron (36). We demonstrated that dendron modification fully unleashed the inherent capability of AFM (36,37). The dendron array on a surface generated by a self-assembly process enables precise control of the spacing between the immobilized biomolecules, and the controlled surface architecture allows a single molecular interaction between a probe on an AFM tip and a target on a substrate.

MATERIALS AND METHODS

General

Dendron-modified glass slides were purchased from NSB Postech Inc. (www.nsbpostech.com). The dendron that was used for the tip modification—(9-anthrylmethyl-3-({[tris({[(1-{tris[(2-{[(tris{[2-carboxyethoxy]methyl}methyl)amino]carbonyl}ethoxy)methyl]methyl} amino)carbonyl]-2-ethoxy}methyl)methyl]amino}carbonyl)propyl-carbamate (or 27-acid dendron)—was purchased from Panagene (www.panagene.com) after its custom order synthesis. The silane coupling agent *N*-(3-(triethoxysilyl)propyl)-*O*-polyethyleneoxide urethane (TPU) was obtained from Gelest. All other chemicals were of reagent grade and were acquired from Sigma-Aldrich. Deionized water (18 MΩ·cm) was obtained by passing distilled water through a Barnstead E-pure 3-Module system. Water used in RNA experiments was pretreated overnight with diethylpyrocarbonate [DEPC, 0.05% (v/v)] and subsequently autoclaved. All DNA oligonucleotides were purchased from Bionics (Korea).

Sample preparation

AFM probe pretreatment

Standard rectangular silicon nitride probes [DPN® Probes, Type B (S-4); NanoInk, Inc.; spring constant (~16 pN/nm)] were oxidized by heating them in a 10% nitric acid solution at 80°C for 20 min. The cantilevers were washed and rinsed thoroughly with a copious amount of deionized water. After oxidation, the cantilevers were dried in a vacuum chamber (30–40 mTorr) for 20 min and used immediately.

Slide cleaning

Bare glass slides were immersed in an alkaline solution (3 l) containing NaOH (300 g), and a reaction bottle containing the solution and slides was incubated at 70°C for 3 min. The slides were washed and rinsed thoroughly with a copious amount of deionized water. The clean slides were dried in a vacuum chamber (30–40 mTorr) for 30 min and used immediately.

Silylation

The clean AFM probes were placed in 20 ml of anhydrous toluene containing TPU (0.20 ml) under a nitrogen atmosphere for 4 h. After silylation, the probes were washed with toluene and baked at 110°C for 30 min. Next, the probes were rinsed thoroughly with toluene and then methanol, and dried under a vacuum (30–40 mTorr). The slide glasses were treated in the same way.

Preparation of dendron-modified probes and slides

To immobilize the dendron molecule, the silylated probes were immersed in a methylene chloride solution (5 ml) premixed with DMF (5 ml) and containing 27-acid dendron (0.0474 g), the coupling agent 1,3-dicyclohexylcarbodiimide (DCC) (0.0612 g), and 4-dimethylaminopyridine (DMAP) (0.00110 g) for 4 h. After the coupling reaction, the probes were rinsed thoroughly with methylene chloride, methanol and water, in that order. Finally, the probes were washed with methanol and dried under a vacuum (30–40 mTorr). The slides were treated in the same way.

9-Anthrylmethyloxycarbonyl group deprotection

The dendron-modified probes were immersed in a methylene chloride solution (37 ml) containing 1.0 M trifluoroacetic acid (TFA, 3 ml), and the solution was stirred for 1 h. After deprotection, the probes were soaked in a methylene chloride solution (20 ml) containing diisopropylethylamine [DIPEA, 20% (v/v), 5 ml] for 10 min. Then, the probes were rinsed thoroughly with methylene chloride and then methanol, and were kept under a vacuum (30–40 mTorr). The slides were treated in the same way.

Preparing N-hydroxysuccinimide (NHS)-modified probes and slides

The deprotected probes were immersed in an acetonitrile solution (5 ml) containing di(*N*-succinimidyl) carbonate (DSC) (0.032 g) and DIPEA (22 µl) for 4 h under nitrogen. After activation, the slides and probes were dipped in a stirred dimethylformamide (DMF) solution for 30 min, washed gently with methanol, and kept under a vacuum (30–40 mTorr). The slides were treated in the same way.

Immobilization of the detection DNA probe on the AFM probes

The above NHS-modified probes were dipped in a DNA solution (20 µM in NSB spotting buffer) for 12 h. The sequence of the 18-mer detection DNA probe is 5′-NH_2-CTA GCC ATG GCG TTA GTA-3′ (GC content 50%). After conjugation, the probes were stirred in DNA hybridization buffer [2× SSPE buffer (pH 7.4) containing 7.0 mM sodium dodecyl sulfate (SDS)] at 37°C for 1 h, and were rinsed thoroughly with water to remove non-specifically bound oligonucleotides. Finally, the AFM probes were dried under a vacuum (30–40 mTorr).

Immobilization of the capture DNA probe on an NHS-modified slide using a microarrayer

Capture probe DNA solution (200 μM) was prepared using the spotting buffer (0.15× SSC, 0.22 M SDS, 14.9 mM betaine, 6.2 mM NaN_3, pH 8.5), and the probe was printed onto the activated slides using a microarrayer (Q-Array Mini; Genetix) in a clean room (class 10 000). The sequence of the 60-mer capture probe is 5′-Cy3-CTT GTG GTA CTG CCT GAT AGG GTG CTT GCG AGT GCC CCG GGA GGT CTC GTA GAC CGT GCA-3′ (GC content 62%). After spotting, the printed slides were kept in a humidity chamber (~85% humidity) at room temperature for 12 h. Subsequently, the slides were placed in DNA hybridization buffer solution [2× SSPE buffer (pH 7.4) containing 7.0 mM SDS) at 37°C for 20 min with stirring and then in water for 1 min to remove non-specifically bound oligonucleotides. Finally, the slide was dried under a vacuum (30–40 mTorr).

Preparation of HCV RNA

HCV RNA, which was single-stranded and 9.6 kb in length, was provided by the Laboratory Corporation of America (LabCorp). To extract HCV, 0.10 ml of plasma containing HCV was combined with 0.20 ml of a guanidinium isothiocyanate–phenol mixture. Following the addition of 0.20 ml of chloroform, samples were vortexed and then centrifuged at 12 000× *g* for 5 min at 16°C. The aqueous phase was collected and added to 3.0 μl of 20 mg/ml glycogen. Nucleic acids were precipitated by the addition of an ethanol/ammonium acetate mixture, stored for 1 h at 4°C, and centrifuged at 23 000× *g* for 15 min at 4°C. The resulting pellet was washed with 70% ethanol, dried, and redissolved in 30 μl of DEPC-treated water containing DTT and RNase inhibitor.

Hybridization of HCV RNA

After denaturing the RNA for 10 min at 95°C, the RNA, in RNA hybridization buffer [50% formamide, 10% dextran sulfate, 1% 100× Denhardt's solution, 250 μg/ml yeast tRNA, 0.3 M NaCl, 20 mM Tris–HCl (pH 8.0), 5 mM EDTA, 10 mM Na_2HPO_4, 1% sarcosyl], was allowed to react with the capture probes on a slide. For this purpose, a 4-well gasket slide (Agilent Technologies) was placed in a chamber kit, and after placing an RNA solution within the gasket, the spotted glass slide was brought into contact with the solution. After tightening the chamber kit, the whole part was heated at 45°C overnight in a hybridization oven (N-Biotek, Inc., Korea). Subsequently, the slide was washed with DNA hybridization buffer solution [2× SSPE buffer (pH 7.4) containing 7.0 mM SDS] at 75°C for 5 min. Then, the slide was washed with SSC buffer solutions (2×, 1× and 0.1×) three times sequentially at 40°C (10 min each).

AFM force measurement

AFM measurements were carried out with a Force Robot 300 automated force spectrometer (JPK Instruments, Germany) using freshly prepared PBS buffer (pH 7.4) at a measurement velocity of 0.70 μm/s. Cantilevers were calibrated in solution before their use by measuring and analysing the thermal fluctuation spectrum (using a built-in program). Adhesion force maps were obtained by processing the force values recorded during the raster scanning of an area of 150 nm × 150 nm or 900 nm × 900 nm. Force–distance curves were typically recorded 10 times for each pixel, and the mean unbinding force was calculated.

RESULTS AND DISCUSSION

Capture and detection probe design

HCV consists of six major genotypes, and their prevalences vary geographically (19). In the USA, 72% of patients with HCV infection have genotype 1, 16–19% have genotype 2, 8–10% have genotype 3 and 1–2% have the other genotypes (38). The 5′ non-coding (5′ NC) region of HCV RNAs of 324–341 bases in length is a highly conserved domain located among the variable domains of full-length HCV RNA (39). Although some variation is found in the non-coding region, three completely invariant sub-domains exist at positions 246–263, 178–199 and 3–65 (Table 1). To detect HCV RNA regardless of variation, detection and capture DNA probes must be designed to interact with the invariant nucleotide sequences. To avoid detachment during the force-based detection, a 60-mer capture DNA whose sequence was complementary to nucleotides 3–62 of the HCV RNA was selected. An 18-mer detection DNA whose sequence was complementary to positions 246–263 of the HCV RNA was employed because this position was expected to be more accessible to the detection probe.

To control the spacing between the capture DNA probes on a solid substrate and the detection DNAs on an AFM tip, a third-generation dendron (27-acid dendron) was introduced on both surfaces before conjugation of the DNAs. In previous studies, we demonstrated that with surface control the 1:1 interaction between DNAs could be enhanced (36), the individual PSAs [prostate-specific antigens] captured on a surface could be counted (40), and that Pax6 mRNA expressed in a mouse embryonic tissue could be imaged (41). As the

Table 1. Sequences of highly conserved domains in the non-coding region

Position	Sequence of HCV RNA	Length (bases)
3–65	5′-U GCA CGG UCU ACG AGA CCU CCC GGG GCA CUC GCA AGC ACC CUA UCA GGC AGU ACC ACA AGG CC-3′	63
178–199	5′-ACU CAC CGG UUC CGC AGA CCA C-3′	22
246–263	5′-U ACU AAC GCC AUG GCU AG-3′	18

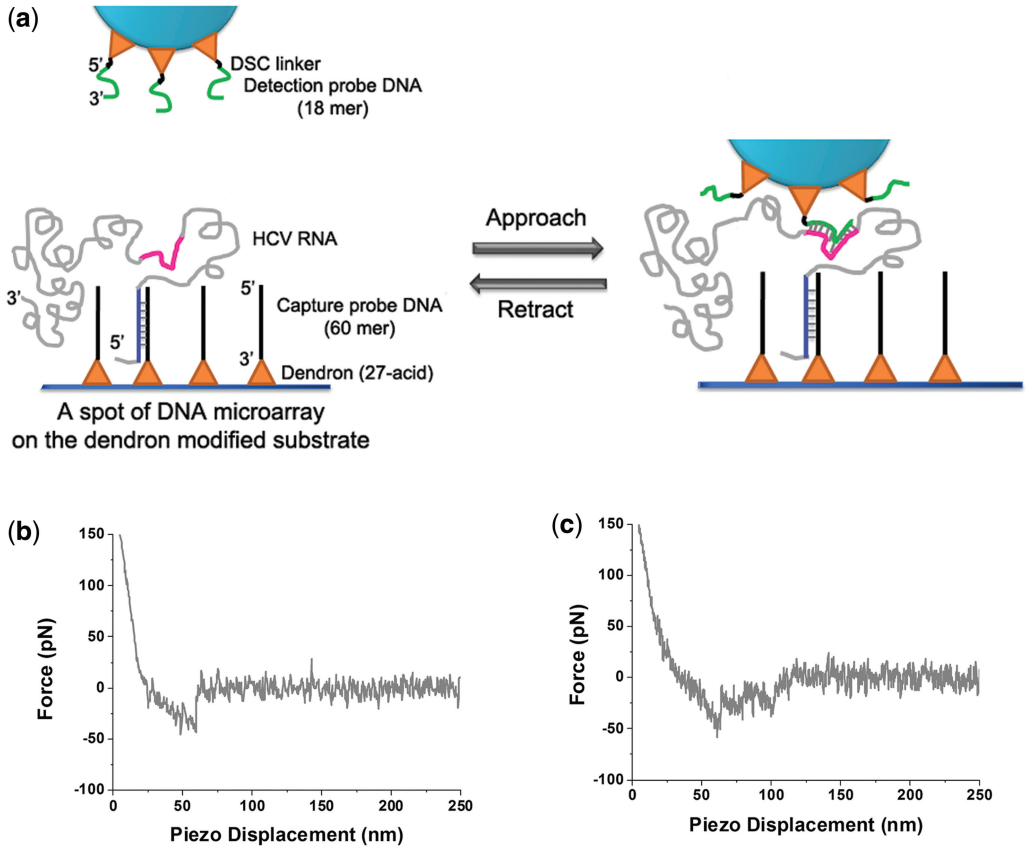

Figure 1. (**a**) Schematic of the experimental setup employed for the force mapping described in this study. Force measurements were recorded at a pulling rate of 0.70 µm/s between the detection DNA and the captured HCV RNA on the surface. The 18-mer detection DNA probe (green) complementary to nucleotides 246–263 of the HCV RNA (pink) was immobilized on the 27-acid dendron-modified AFM tip. The 60-mer capture probe DNA complementary to nucleotides 3–62 of the HCV RNA (blue) was immobilized on a 27-acid dendron-modified silicon substrate. Typical force–distance curve with (**b**) a single rupture and (**c**) multiple ruptures between the detection probe DNA and the complementary part of the HCV RNA.

first step, the capture probe DNA (black), with an amine group at its 3′ end, was covalently linked to the apex of the dendron immobilized on the slide, whereas the detection DNA (green), with an amine group at its 5′ end, was covalently linked to the apex of the dendron immobilized on the AFM tip. Then, HCV RNAs were hybridized with the capture probe DNAs immobilized on the dendron-coated slide (Figure 1a). After hybridization, an AFM probe tethering the detection DNAs was used to measure the interaction with the captured RNAs. Force maps were generated by measuring the force within a designated area at a certain spatial pixel size.

Force–distance curves

When the AFM probe tethering the detection DNAs scanned a certain area within a microarrayed spot, specific curves for the unbinding force between the detection DNA probe and the captured HCV RNA were obtained. A representative force–distance curve is shown in Figure 1b and c. The curve shows a non-linear profile in the retract trace corresponding to extension of the DNA–RNA complex and flexible organic components (including the linker and the dendron) prior to the bond rupture event.

Both single-peak curves (Figure 1b) and multiple-peak curves (Figure 1c) were observed. The multiple peaks could be explained by unwinding of various domains of the secondary structure. Additional interactions with a neighboring RNA is possible, but only when the neighboring RNA is in close proximity. The HCV RNA molecule is single-stranded, but forms 3D secondary structures due to hairpin formation. For the calculation (http://rna.tbi.univie.ac.at/cgi-bin/RNAfold.cgi), a part of the 5′ NC region (nucleotides 3–263) was considered because only this part will be stretched during retraction (Figure 2). Although form A is more stable than form B, the two forms are expected to coexist because the largest energy difference is 1.6 kcal/mol. Therefore, the shapes of the force–distance curves for DNA and HCV RNA were expected to be complicated.

To obtain the force value distribution, the force was measured for a substrate hybridized with a HCV RNA sample (6.0 fM). From 9000 data points (four areas, 225 points per area; 10 times per point; Figure 3a–d), 295 specific curves were noted. The mean force value was 32 ± 5 pN (force value ± σ; the most probable force value = 31 ± 5 pN; Figure 4a). The mean rupture force value for DNA and HCV RNA was close to the reference

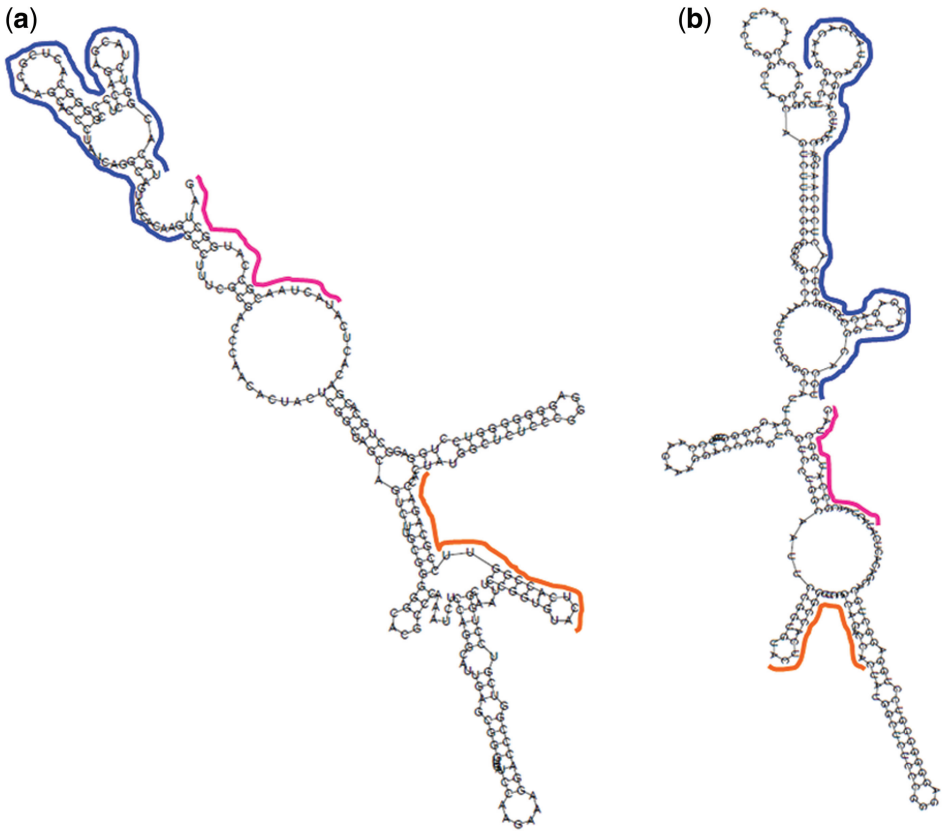

Figure 2. Secondary structures of 5′ non-coding region (nucleotides 3–263) of HCV RNA (http://rna.tbi.univie.ac.at/cgi-bin/RNAfold.cgi). There are two major RNA secondary structures of which minimum free energy is (**a**) −98.95 kcal/mol and (**b**) −97.30 kcal/mol, respectively. Three sub-domains that were completely invariant among seven major genotypes of HCV RNA were indicated by blue (positions from 3 to 65), orange (positions from 178 to 199) and pink (positions 246 to 263).

value (35 pN) obtained previously for short DNA–short RNA (41). The corresponding unbinding distance ranged from 8 nm to 70 nm (Figure 4b). This wide range can be explained by the coexistence of two RNA structures and variation in the unfolding state at the end of the detachment. The calculated stretching distance of HCV RNA ranged from 45 nm to 80 nm (Supplementary Data). Although a stretching distance of 80 nm was observed in the maps, the distance was typically shorter than this maximum value. Rupture distances shorter than the maximal value reflect the fact that the duplex formed between the detection DNA and HCV RNA is ruptured before full stretching, and the contact point is not at the center.

2D mapping

Maps with pixel size of 10 nm showed an individual captured target HCV RNA. The example in Figure 3a shows that the hydrodynamic distance was 50–60 nm. Twenty-three pixels within the box show the specific unbinding curves. The probability of obtaining the specific curve was 70–90% at the center and 10–40% near the boundary. Apart from one pixel (the purple pixel) the mean force ranged from 22 pN to 42 pN (yellow pixels). Examination of four other clusters showed that 73 pixels within the boxes were within the above force range and that the hydrodynamic distance was 30–60 nm (Figure 3b–d). To map a larger area, the pixel size was adjusted to 20 nm so that the map did not miss any captured RNA and a specific site came as a cluster of pixels (no fewer than two). The adhesion force curves were recorded ten times per pixel at the interval across a selected area (900 nm × 900 nm; Figure 3e). To create a map for HCV RNA distribution, curves with no events or linear profiles were deleted using a JPK data processing program, and the remaining curves were validated one by one. For example, for the 5.7 fM sample, 200 curves remained after filtering, and pixels for the remaining curves were displayed (Figure 3e). For clarity, 29 pixels of 10% probability were not displayed in the map. These pixels did not affect the counting because they were all isolated (in other words, they did not form clusters, which will be discussed later). The averaged probability of the cluster-forming yellow pixels was 46%. The mean force value of each pixel was calculated, and pixels showing the specific event were categorized according to the mean force. Five purple pixels (force $\geq$ 43 pN), 34 yellow pixels (22–42 pN) and two gray pixels ($\leq$21 pN) were noted, along with 1862 no-event pixels and 93 non-specific-event pixels. All these pixels were colored black.

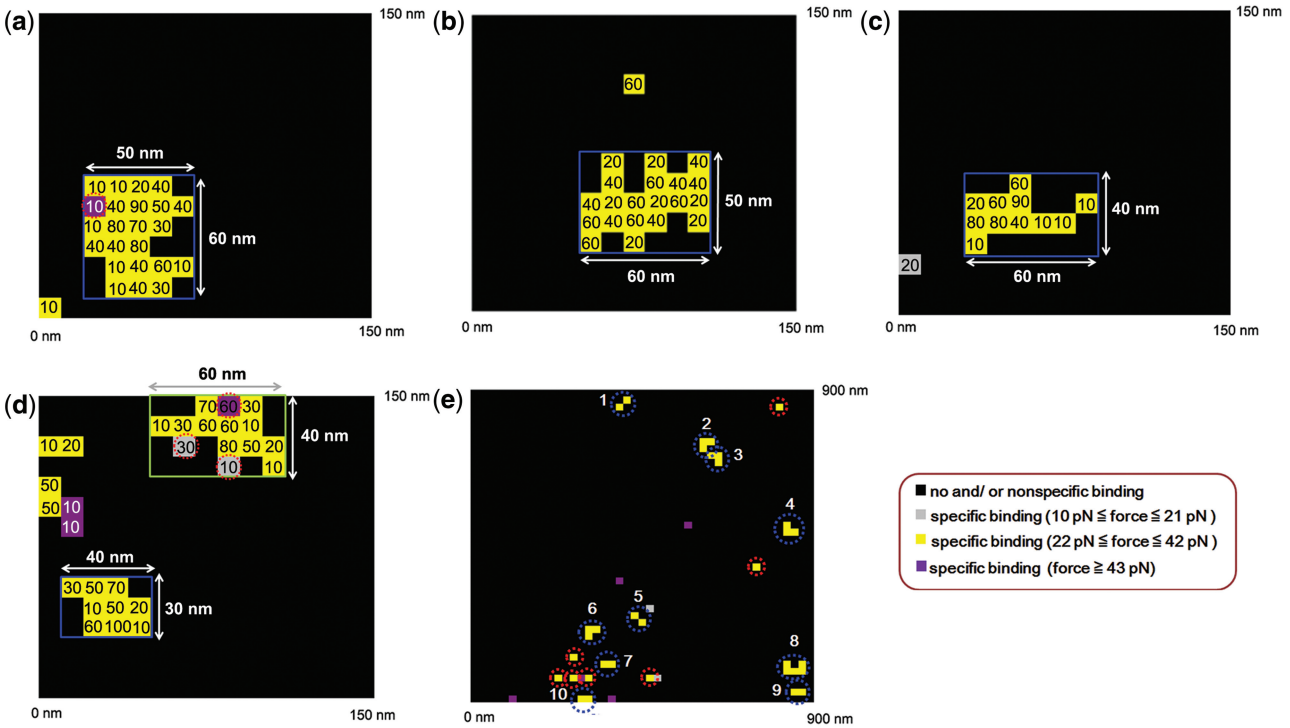

Figure 3. (**a–d**) Force–distance curves for target HCV RNA (6.0 fM) were recorded within a 150 nm × 150 nm area with a lateral pixel size of 10 nm. The number in each pixel represents the percentage of getting the specific event. The diameter of the clusters was within 30–60 nm. The pixels with the red circle showed the mean value out of the range (22–42 pN). (**e**) Adhesion force map of a 900 nm × 900 nm area with a lateral pixel size of 20 nm, obtained using target HCV RNA (5.7 fM). Mean force values were categorized into four levels, indicated by different colors. Isolated pixels are marked with red circles and clusters with blue circles.

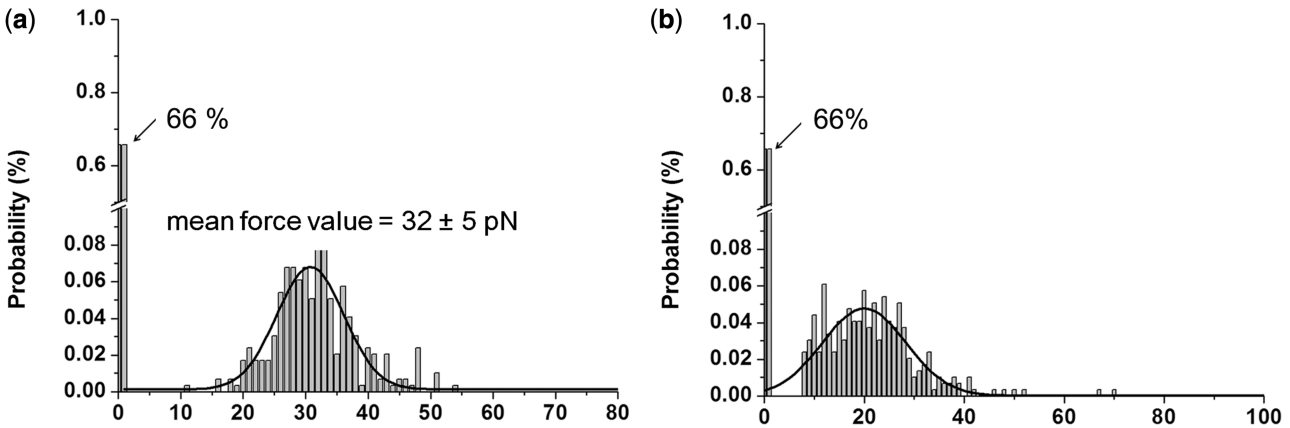

Figure 4. The histograms of the unbinding force (**a**) and the distance (**b**) derived from the force–distance curves of the interaction recorded on an area (150 nm × 150 nm) for a sample of 6.0 fM HCV RNA. The mean value of unbinding force was 32 ± 5 (the force value ± σ) pN (a) and the unbinding distance ranged from 8 nm to 70 nm (b). The probability of getting the specific event was 34%.

Assigning individual RNAs in a map

To assign individual HCV RNAs, only clusters consisting of two or more yellow pixels (marked by a blue circle) were counted; the isolated pixels (marked by a red circle in Figure 3e and Supplementary Figure S1) were not counted. The smaller (gray) and larger (purple) force values are believed to have originated from the interaction between the detection probe DNA and other competing non-HCV RNAs. Also, note that these pixels are mostly non-cluster-forming. In some cases, two clusters are close to each other, and care should be taken to achieve the correct assignment. For example, the six neighboring pixels (top middle) were grouped into two clusters (numbers 2 and 3 in Figure 3e) because the longest length was 80 nm. However, some ambiguity must be acknowledged when grouping the five neighboring pixels (number 8; bottom right). Nevertheless, they were counted as a cluster because the longest length (60 nm) was within the range observed in the maps with pixel size of 10 nm.

Table 2. Count number of the cluster versus concentration

Concentration (fM)	Count number	Spot diameter (μm)	Normalized count number (number per 200 μm)	Average normalized value (SD)
6.0	15	164	10.1	10.8 (1.2)
	15			
	14	189	12.5	
	10	203	10.3	
5.7	10	202	10.2	10.3 (0.06)
	11	198	10.3	
	10			
4.3	10	203	9.8	8.1 (1.9)
	9			
	9	204	7.8	
	6			
	5	203	5.2	
2.6	6	185	6.0	5.4 (0.9)
	8			
	6	204	5.7	
	5			
	3	226	3.8	
0.76	4	201	3.0	2.3 (0.9)
	2			
	2	202	1.5	
	1			

Allowing a 10% error in the assigning process is safe, and the error is frequently close to the variation obtained from multiple runs.

Cluster number versus concentration

To count the captured RNAs at various concentrations, two or three microarrayed spots were examined for each concentration (6.0, 5.7, 4.3, 2.6 and 0.76 fM), and one or two maps were generated for each to consider the variation within and among spots. To minimize the variation within spots, HCV RNA adhesion force maps were recorded around the center of the spots at each measurement. Nevertheless, a certain amount of variation occurred within spots (e.g. 9 versus 6 at 4.3 fM, 6 versus 8 at 2.6 fM and 4 versus 2 at 0.76 fM). One must normalize the average cluster numbers to a standard diameter (200 μm) because a larger area yields a smaller cluster number at a fixed concentration (Table 2). The normalized values showed variation at a fixed concentration (10.1–12.5 for 6.0 fM, 10.2–10.3 for 5.7 fM, 5.2–9.8 for 4.3 fM, 3.8–6.0 for 2.6 fM and 1.5–3.0 for 0.76 fM). The average count numbers were 10.8, 10.3, 8.1, 5.4 and 2.3 at concentrations of 6.0, 5.7, 4.3, 2.6 and 0.76 fM, respectively. The relationship between average count number and RNA concentration is shown in Figure 5. The open circles represent the normalized values, the error bars indicate the standard deviation and the filled squares show the averaged normalized values. A fairly good linear correlation ($r = 0.999$) was observed between averaged normalized value and RNA concentration. The filled triangles represent the calculated count number, whose value was consistently smaller than the observed one. The solid and broken lines are parallel. The difference with respect to the observed values was 14% at 6.0 fM and 48% at 0.76 fM. The difference may have been due to an error in the mapping and cluster counting and/or inaccuracy in the concentration determined by reverse transcription and PCR. To understand the difference, investigating more samples of lower concentration including 0.76 fM is necessary.

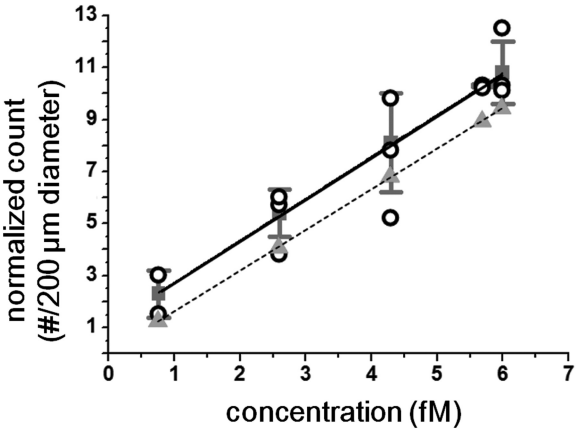

Figure 5. Relationship between the average normalized count number and RNA concentration (copy number). A good linear correlation ($r = 0.999$) was noted. The open circles represent normalized values, the error bar indicates the standard deviation, and the filled squares show the averaged normalized values. The filled triangles represent the calculated count number, the value of which was consistently smaller than the observed one. The solid and broken lines are parallel.

With the current format (spot diameter 2×10^2 μm, scan area 900 nm × 900 nm), the lowest detectable concentration of HCV RNA was 0.76 fM. The detection limit is expected to decrease when the spot size is reduced or a larger area is scanned at the same pixel size. Because few established approaches exist for obtaining small spots (1–10 μm), including polymer pen lithography and microcontact printing, enhancing the detection limit by a factor of 100 or 10 000 can be envisaged. The projected detection limit when the whole area of a 1.0-μm spot is examined is several tens of zM (<10 copies).

CONCLUSIONS

Force-based AFM was used to analyse captured HCV RNAs on a surface. The advantages of this approach are the lack of need for labeling, modification, reverse transcription and amplification. By utilizing dendron self-assembly on the surface, one was able to obtain a mostly 1:1 interaction between the detection DNA on the AFM tip and the captured RNA. While the force–distance curves showed single and multistep stretches reflecting unfolding of the secondary structures, the specific force value, probability of obtaining the specific curve, and stretching distance were useful criteria in generating the force map. Maps with pixel size of 10 nm and 20 nm were obtained; the map with former pixel size provided information about the hydrodynamic distance. The number of clusters in the map showed a linear relationship with the concentration of RNA, and the lowest detectable RNA concentration in the current format was

0.76 fM. The difference between the observed number and the calculated one increased at low concentrations. Although the current detection limit (0.76 fM) is insufficient for the clinical application, utilizing AFM in combination with smaller spots (1–10 μm) seems promising.

SUPPLEMENTARY DATA

Supplementary Data are available at NAR Online: Supplementary Figure 1, Supplementary Data and Supplementary References [42–46].

FUNDING

The World Class University (WCU) program through the National Research Foundation (NRF) of Korea funded by the Ministry of Education, Science and Technology (MEST) [R31-2008-000-10105-0, 2012-0001135] and [BK21]. Funding for open access charge: NRF of Korea funded by the MEST [2012-0001135].

Conflict of interest statement. None declared.

REFERENCES

1. Urdea,M., Penny,L.A., Olmsted,S.S., Giovanni,M.Y., Kaspar,P., Shepherd,A., Wilson,P., Dahl,C.A., Buchsbaum,S., Moeller,G. *et al*. (2006) Requirements for high impact diagnostics in the developing world. *Nature*, **444**, 73–79.
2. Mabey,D., Peeling,R.W., Ustianowski,A. and Perkins,M.D. (2004) Tropical infectious diseases: diagnostics for the developing world. *Nat. Rev. Microbiol.*, **2**, 231–240.
3. Hood,L., Heath,J.R., Phelps,M.E. and Lin,B. (2004) Systems biology and new technologies enable predictive and preventative medicine. *Science*, **306**, 640–643.
4. Yager,P., Edwards,T., Fu,E., Helton,K., Nelson,K., Tam,M.R. and Weigl,B.H. (2006) Microfluidic diagnostic technologies for global public health. *Nature*, **442**, 412–418.
5. Lee,H., Sun,E., Ham,D. and Weissleder,R. (2008) Chip-NMR biosensor for detection and molecular analysis of cells. *Nat. Med.*, **14**, 869–874.
6. Wulfkuhle,J.D., Liotta,L.A. and Petricoin,E.F. (2003) Proteomic applications for the early detection of cancer. *Nat. Rev. Cancer*, **3**, 267–275.
7. Choo,Q.L., Kuo,G., Weiner,A.J., Overby,L.R., Bradley,D.W. and Houghton,M. (1989) Isolation of a cDNA clone derived from a blood-borne non-A, non-B viral hepatitis genome. *Science*, **244**, 359–362.
8. Heller,T., Saito,S., Auerbach,J., Williams,T., Moreen,T.R., Jazwinski,A., Cruz,B., Jeurkar,N., Sapp,R., Luo,G. *et al*. (2005) An *in vitro* model of hepatitis C virion production. *Proc. Natl Acad. Sci. USA*, **102**, 2579–2583.
9. Patel,K., Albrecht,J., Owens,E., Dev,A., Heaton,S., Pianko,S., Pockros,P.J., Conrad,A., Blatt,L.M. and McHutchison,J.C. (2005) The clinical utility of using Catrimox-14-treated whole blood in detecting hepatitis C virus RNA. *Antivir. Ther.*, **10**, 535–541.
10. Martell,M., Briones,C., de Vicente,A., Piron,M., Esteban,J.I., Esteban,R., Guardia,J. and Gómez,J. (2004) Structural analysis of hepatitis C RNA genome using DNA microarrays. *Nucleic Acids Res.*, **32**, e90.
11. Wilkins,T., Malcolm,J.K., Raina,D. and Schade,R.R. (2010) Hepatitis C: diagnosis and treatment. *Am. Fam. Physician*, **81**, 1351–1357.
12. Liang,T.J., Rehermann,B., Seeff,L.B. and Hoofnagle,J.H. (2000) Pathogenesis, natural history, treatment, and prevention of hepatitis C. *Ann. Intern. Med.*, **132**, 296–305.
13. Shiffman,M.L. (2011) *Chronic Hepatitis C Virus: Advances in Treatment, Promise for the Future*. Springer, New York, NY, USA.
14. Cotler,S.J., Reddy,K.R., McCone,J., Wolfe,D.L., Liu,A., Craft,T.R., Ferris,M.W., Conard,A.J., Albrecht,J., Morrissey,M. *et al*. (2001) An analysis of acute changes in interleukin-6 levels after treatment of hepatitis C with consensus interferon. *J. Interferon Cytokine Res.*, **21**, 1011–1019.
15. McHutchison,J.G. (2004) Understanding hepatitis C. *Am. J. Manag. Care*, **10**, S21–S29.
16. Nelson,P.K., Mathers,B.M., Cowie,B., Hagan,H., Des Jarlais,D., Horyniak,D. and Degenhardt,L. (2011) Global epidemiology of hepatitis B and hepatitis C in people who inject drugs: results of systematic reviews. *Lancet*, **378**, 571–583.
17. Jou,J.H. and Muir,A.J. (2008) Hepatitis C. *Ann. Intern. Med.*, **148**, ITC6–1–ITC6-16.
18. Terrault,N.A., Pawlotsky,J.M., McHutchison,J., Anderson,F., Krajden,M., Gordon,S., Zitron,I., Perrillo,R., Gish,R., Holodniy,M. *et al*. (2005) Clinical utility of viral load measurements in individuals with chronic hepatitis C infection on antiviral therapy. *J. Viral Hepat.*, **12**, 465–472.
19. Rosen,H.R. (2011) Chronic hepatitis C infection. *N. Engl. J. Med.*, **364**, 2429–2438.
20. Griffin,J., Singh,A.K., Senapati,D., Lee,E., Gaylor,K., Jones-Boone,J. and Ray,P.C. (2009) Sequence-specific HCV RNA quantification using the size-dependent nonlinear optical properties of gold nanoparticles. *Small*, **5**, 839–845.
21. Sarrazin,C., Gartner,B.C., Sizmann,D., Babiel,R., Mihm,U., Hofmann,W.P., von Wagner,M. and Zeuzem,S. (2006) Comparison of conventional PCR with real-time PCR and branched DNA-based assays for hepatitis C virus RNA quantification and clinical significance for genotypes 1 to 5. *J. Clin. Microbiol.*, **44**, 729–737.
22. Hendricks,D.A., Friesenhahn,M., Tanimoto,L., Goergen,B., Dodge,D. and Comano,L. (2003) Multicenter evaluation of the VERSANT HCV RNA qualitative assay for detection of hepatitis C virus RNA. *J. Clin. Microbiol.*, **41**, 651–656.
23. Sarrazin,C. (2002) Highly sensitive hepatitis C virus RNA detection methods: molecular backgrounds and clinical significance. *J. Clin. Virol.*, **25**, S23–S29.
24. Tsongalis,G.J. (2006) Branched DNA technology in molecular diagnostics. *Am. J. Clin. Pathol.*, **126**, 448–453.
25. Seeman,N.C. (1991) The use of branched DNA for nanoscale fabrication. *Nanotechnology*, **2**, 149–159.
26. Clarke,L.A., Rebelo,C.S., Gonçalves,J., Boavida,M.G. and Jordan,P. (2001) PCR amplification introduces errors into mononucleotide and dinucleotide repeat sequences. *Mol. Pathol.*, **54**, 351–353.
27. Bustina,S.A. and Nolanb,T. (2004) Pitfalls of quantitative real-time reverse-transcription polymerase chain reaction. *J. Biomol. Tech.*, **15**, 155–166.
28. Piyamongkol,W., Bermúdez,M.G., Harper,J.C. and Wells,D. (2003) Detailed investigation of factors influencing amplification efficiency and allele drop-out in single cell PCR: implications for preimplantation genetic diagnosis. *Mol. Hum. Reprod.*, **9**, 411–420.
29. Zhang,W., Lü,X., Zhang,W.K. and Shen,J. (2011) EMSA and single-molecule force spectroscopy study of interactions between *Bacillus subtilis* single-stranded DNA-binding protein and single-stranded DNA. *Langmuir*, **27**, 15008–15015.
30. Kienberger,F., Ebner,A., Gruber,H.J. and Hinterdorfer,P. (2006) Molecular recognition imaging and force spectroscopy of single biomolecules. *Acc. Chem. Res.*, **39**, 29–36.
31. Li,H., Oberhauser,A.F., Fowler,S.B., Clarke,J. and Fernandez,J.M. (2000) Atomic force microscopy reveals the mechanical design of a modular protein. *Proc. Natl Acad. Sci. USA*, **97**, 6527–6531.
32. Müller,D.J., Helenius,J., Alsteens,D. and Dufrêne,Y.F. (2009) Force probing surfaces of living cells to molecular resolution. *Nat. Chem. Biol.*, **5**, 383–390.
33. Rankla,S., Kienbergerb,F., Wildlinga,L., Wrussc,J., Grubera,H.J., Blaasc,D. and Hinterdorfer,P. (2008) Multiple receptors involved in human rhinovirus attachment to live cells. *Proc. Natl Acad. Sci. USA*, **105**, 17778–17783.

34. Husale,S., Persson,H.H.J. and Sahin,O. (2009) DNA nanomechanics allows direct digital detection of complementary DNA and microRNA targets. *Nature*, **462**, 1075–1078.
35. Hong,B.J., Oh,S.J., Youn,T.O., Kwon,S.H. and Park,J.W. (2005) Nanoscale-controlled spacing provides DNA microarrays with the SNP discrimination efficiency in solution phase. *Langmuir*, **21**, 4257–4261.
36. Jung,Y.J., Hong,B.J., Zhang,W., Tendler,S.J.B., Williams,P.M., Allen,S. and Park,J.W. (2007) Dendron arrays for the force-based detection of DNA hybridization events. *J. Am. Chem. Soc.*, **129**, 9349–9355.
37. Kim,I.H., Lee,H.Y., Lee,H.D., Jung,Y.J., Tendler,S.J.B., Williams,P.M., Allen,S., Ryu,S.H. and Park,J.W. (2009) Interactions between signal-transducing proteins measured by atomic force microscopy. *Anal. Chem.*, **81**, 3276–3284.
38. McHutchison,J.G., Gordon,S.C., Schiff,E.R., Shiffman,M.L., Lee,W.M., Rustgi,V.K., Goodman,Z.D., Ling,M.H., Cort,S. and Albrecht,J.K. (1998) Interferon alfa-2b alone or in combination with ribavirin as initial treatment for chronic hepatitis C. Hepatitis Interventional Therapy Group. *N. Engl. J. Med.*, **339**, 1485–1492.
39. Bukh,J., Purcell,R.H. and Miller,R.H. (1992) Sequence analysis of the 5′ noncoding region of hepatitis C virus. *Proc. Natl Acad. Sci. USA*, **89**, 4942–4946.
40. Roy,D., Kwon,S.H., Kwak,J.-W. and Park,J.W. (2010) Seeing and counting individual antigens captured on a microarrayed spot with force-based atomic force microscopy. *Anal. Chem.*, **82**, 5189–5194.
41. Jung,Y.J., Park,Y.S., Yoon,K.-J., Kong,Y.-Y., Park,J.W. and Nam,H.G. (2009) Molecule-level imaging of Pax6 mRNA distribution in mouse embryonic neocortex by molecular interaction force microscopy. *Nucleic Acids Res.*, **37**, e10.
42. Lambert,M.N., Vöcker,E., Blumberg,S., Redemann,S., Gajraj,A., Meiners,J.-C. and Walter,N.G. (2006) Mg^{2+}-induced compaction of single RNA molecules monitored by tethered particle microscopy. *Biophys. J.*, **90**, 3672–3685.
43. Kufer,S.K., Strackharn,M., Stahl,S.W., Gumpp,H., Puchner,E.M. and Gaub,H.E. (2009) Optically monitoring the mechanical assembly of single molecules. *Nat. Nanotechnol.*, **4**, 45–49.
44. Liphardt,J., Onoa,B., Smith,S.B., Tinoco,I. Jr and Bustamante,C. (2001) Reversible unfolding of single RNA molecules by mechanical force. *Science*, **292**, 733–737.
45. Onoa,B., Dumont,S., Liphardt,J., Smith,S.B., Tinoco,I. Jr and Bustamante,C. (2003) Identifying kinetic barriers to mechanical unfolding of the *T. thermophila* ribozyme. *Science*, **299**, 1892–1895.
46. Green,N.H., Williams,P.M., Wahab,O., Davies,M.C., Roberts,C.J., Tendler,S.J.B. and Allen,S. (2004) Single-molecule investigations of RNA dissociation. *Biophys. J.*, **86**, 3811–3821.